

**Giant magnetocaloric effect and hysteresis loss in $\text{Mn}_x\text{Fe}_{2-x}\text{P}_{0.5}\text{Si}_{0.5}$ ($0.7 \leq x \leq 1.2$)
microwires at ambient temperatures**

Lin Luo¹, Hongxian Shen^{1,*}, Lunyong Zhang¹, Yongjiang Huang¹, Jianfei Sun^{1,*},
and Manh-Huong Phan^{2,*}

¹ School of Materials Science and Engineering, Harbin Institute of Technology, Harbin
150001, China

²Department of Physics, University of South Florida, Tampa, FL 33620, USA

Magnetocaloric microwires are very promising for energy-efficient magnetic refrigeration in micro electromechanical systems (MEMS) and nano electromechanical systems (NEMS). Creating microwires that exhibit large magnetocaloric effects around room temperature represents an important but challenging task. Here, we report a tunable giant magnetocaloric effect around room temperature in $\text{Mn}_x\text{Fe}_{2-x}\text{P}_{0.5}\text{Si}_{0.5}$ ($0.7 \leq x \leq 1.2$) microwires by utilizing a melt-extraction technique paired with thermal treatment and chemical engineering. The isothermal magnetic entropy change (ΔS_{iso}) and Curie temperature (T_C) can be tuned by adjusting the Mn/Fe ratio. The T_C varies from 351 to 190 K as x increases from 0.8 to 1.2. Among the compositions investigated, the $x = 0.9$ sample shows the largest value of $\Delta S_{\text{iso}} = 18.3 \text{ J kg}^{-1} \text{ K}^{-1}$ for a field change of 5 T around 300 K. After subtracting magnetic hysteresis loss, a large refrigerant capacity of $\sim 284.6 \text{ J kg}^{-1}$ is achieved. Our study paves a new pathway for the design of novel magnetocaloric microwires for active magnetic refrigeration at ambient temperatures.

Keywords: MnFePSi microwires, melt-extraction, magnetocaloric effect, magnetic

refrigeration

*Corresponding authors: jfsun@hit.edu.cn (Jianfei Sun); hitshenhongxian@163.com

(Hongxian Shen); phanm@usf.edu (Manh-Huong Phan)

Introduction

Solid-state magnetic refrigeration has attracted a great deal of attention due to its high energy efficiency and environmental friendliness.^[1,2] In the past decades, many studies have focused on exploring magnetocaloric materials which are crucial components (also known as magnetic beds) in magnetic refrigerators.^[3,4] However, current refrigerators operate at relatively low frequencies (up to a few ten Hertz), thus limiting the overall cooling efficiency.^[5,6] Theoretical studies have suggested that the cooling efficiency of a magnetic refrigerator can be enhanced by optimizing the shape of the magnetocaloric materials used.^[7,8] It has been predicted that a magnetic bed composed of magnetocaloric wires (e.g., Gd wires) yields an optimal device performance, as compared to their powder or laminate structures.^[8] Owing to their increased surface-to-volume area, magnetocaloric wires also promise to promote a higher heat transfer between the magnetic refrigerant and a surrounding liquid. To realize these predictions, a large class of Gd-alloy microwires has been fabricated by the melt-extraction technique, and their magnetic and magnetocaloric properties have been extensively studied in recent years.^[9-15] Due to their Curie temperature (T_C) regime being limited to the nitrogen temperature, however, the Gd-based microwires are only suited for magnetic refrigeration as nitrogen liquefaction.^[11,15] Efforts to tune the magnetocaloric effect from nitrogen to room temperature have been made with little success.^[16-19] While the Curie

temperature appeared to be tunable, to some extent, by varying chemical compositions, the magnetic entropy change (ΔS_{iso}) was found to decrease in Gd-based microwires with enhanced Curie temperatures.^[11,15] This represents an important but challenging task in the field.

Among the magnetocaloric materials explored, Mn-Fe-P-Si alloys have been shown to exhibit a giant magnetocaloric effect around room temperature.^[20,21] In addition to this outstanding property, the low cost of the material with no use of expensive or critical elements makes it one of the most promising refrigerants for large-scale cooling utilization. From the material engineering perspective, however, it is challenging to create Mn-Fe-P-Si alloys with high fractions of desirable Fe_2P phase. Previous studies have shown that time-consuming heat-treatment (up to several days or months) at high temperature is needed to form a high volume fraction of the Fe_2P phase, as well as to achieve compositionally homogeneous Mn-Fe-P-Si, using conventional methods.^[22-24] This makes the total cost of producing the material much higher. Recently, rapid solidification such as melt-extraction technology has been employed to prepare Mn-Fe-P-Si microwires, which significantly reduces the heat treatment duration.^[25] An elevated amount of the Fe_2P phase was achieved, which could be increased following short-time (only 15 min) annealing. Compared to its as-quenched state, a two-fold increase in ΔS_{iso} was achieved in thermally treated Mn-Fe-P-Si microwires.^[8] It is worth pointing out that the magnetic and magnetocaloric properties of Fe_2P -based materials are sensitive to changes in their composition and microstructures.^[26,27] Mn-Fe-P-Si alloys prepared by different techniques were reported to yield uncontrollable chemical compositions resulting in low volume-fractions of the Fe_2P phase.^[28,29] Adjusting the Mn/Fe ratio appears to be crucial to tailor the composition and microstructure of Mn-Fe-P-Si, to improve its magnetocaloric

response.

In this work, we aimed to harness melt-extraction technology with thermal treatment and chemical engineering to create Mn-Fe-P-Si microwires with large, tunable ΔS_{iso} and T_C values at ambient temperatures. We systematically investigated the effect of varying the Mn/Fe ratio on the microstructure and magnetocaloric properties, as well as thermal and magnetic hysteresis losses of $\text{Mn}_x\text{Fe}_{2-x}\text{P}_{0.5}\text{Si}_{0.5}$ ($0.7 \leq x \leq 1.2$) microwires. We have found that the $x = 0.9$ sample possesses the largest ΔS_{iso} value of $\sim 18.3 \text{ J kg}^{-1} \text{ K}^{-1}$ for a field change of 5 around 300 K. A high refrigerant capacity of $\sim 284.6 \text{ J kg}^{-1}$ after subtracting the magnetic hysteresis loss is also achieved. Our study provides an effective approach for designing microwires with novel magnetocaloric properties for application in solid-state cooling systems at ambient temperatures.

Results and Discussion

Microstructural characterization

The XRD patterns of $\text{Mn}_x\text{Fe}_{2-x}\text{P}_{0.5}\text{Si}_{0.5}$ ($0.7 \leq x \leq 1.2$) microwires at room temperature revealed a hexagonal Fe_2P -type structure (space group $P\bar{6}2m$) in addition to an impurity $(\text{MnFe})_3\text{Si}$ (space group $Fm\bar{3}m$) phase, as shown in Fig. 1(a). Tegus *et al.* [31] analyzed the XRD patterns of Fe_2P -type Mn-Fe-P-As compounds and concluded that the XRD patterns could be indexed with the Fe_2P structure type, and the Fe_2P -type compounds underwent a paramagnetic to ferromagnetic transition as the overlapping (211) and (002) peaks became separated. Wang *et al.* also have suggested that the well-separating (211) and (002) peaks bear the ferromagnetic (FM) characteristic of the Fe_2P phase, while the overlapping (211) and (002) peaks imply the paramagnetic (PM) nature of the Fe_2P phase. [32] According to the XRD patterns collected at

ambient temperature (Fig. 1a), it can be inferred that the Fe_2P phase is FM for $x=0.7$ but PM for $x \geq 0.9$, whereas two phases coexist for $x=0.8$.

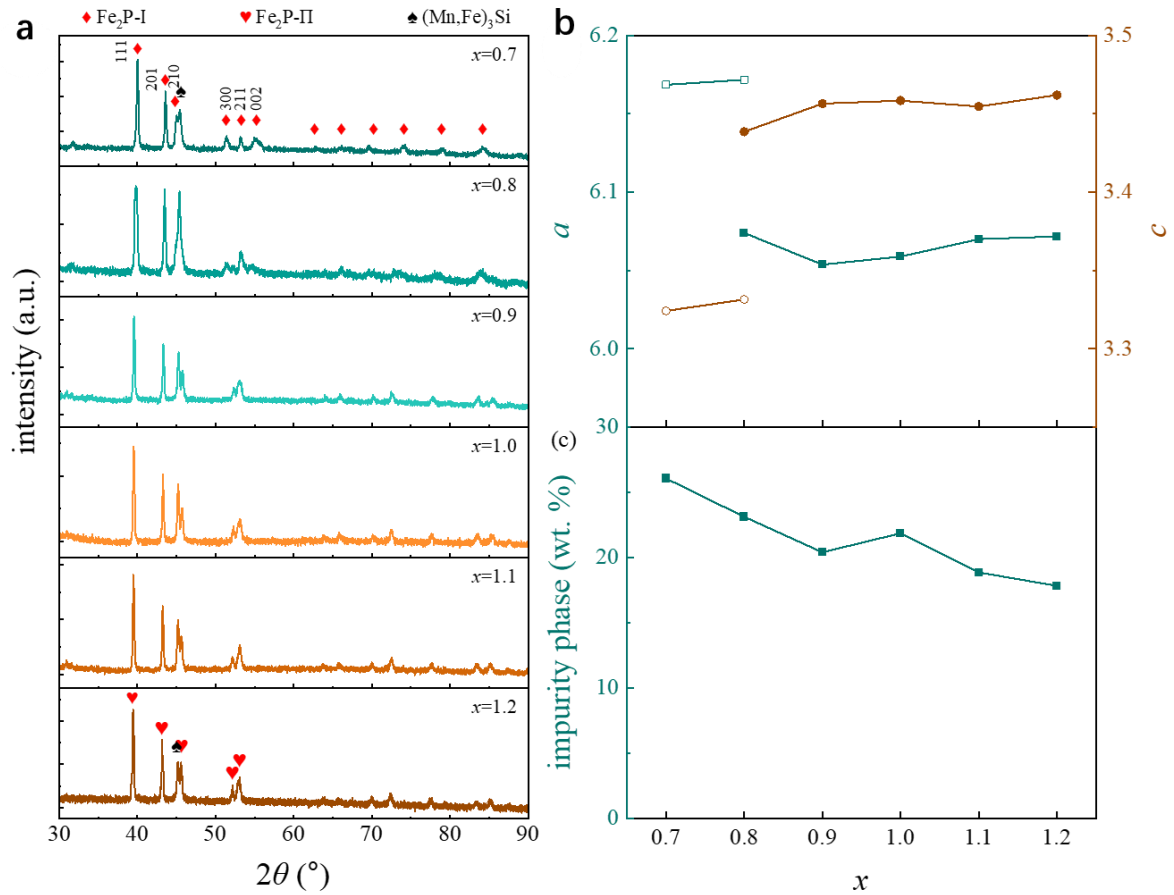


Fig. 1. (a) The room temperature XRD patterns and (b, c) Rietveld refinement results of the lattice constants and impurity phase fraction of $\text{Mn}_x\text{Fe}_{2-x}\text{P}_{0.5}\text{Si}_{0.5}$ microwires as the Mn content is varied. Lattice parameters (a and c) are in Å.

The Rietveld refinement results, as shown in Fig.1(b) and (c), provide further support to the conclusion drawn by the XRD patterns. As shown in Fig. 2(a), the FM Fe_2P phase for $x=0.7$ shows a larger lattice a and a smaller c than the PM Fe_2P phase for $x \geq 0.9$. Both the PM and FM phases coexist for $x=0.8$. In addition, the amount of impurity phase $(\text{Mn,Fe})_3\text{Si}$ decreased as the Mn content x increased. The decrease of the $(\text{Mn,Fe})_3\text{Si}$ phase could be attributed to the decrease of Fe content.

The SEM images (Backscatter Electron mode) and the EDS analysis results of the cross section for a representative sample $\text{Mn}_{1.0}\text{Fe}_{1.0}\text{P}_{0.5}\text{Si}_{0.5}$ are shown in Fig. 2. The impurity visible in light gray zone is observed as a long strip shape or oval shape. The EDS maps clearly show that P is rich in the main phase and almost negligible in the impurity phase. Furthermore, the EDS line scans indicate that more Mn atoms entered the main phase, while more Fe and Si atoms entered the impurity phase. The compositions of these two phases in $\text{Mn}_x\text{Fe}_{2-x}\text{P}_{0.5}\text{Si}_{0.5}$ microwires were analyzed by EDS, which are listed in Table 1. The above results further specify that the main phase is 2:1 and the impurity phase is 3:1. Accordingly, it is understandable that the composition of the Fe_2P phase deviates from its nominal composition due to the presence of the $(\text{Mn,Fe})_3\text{Si}$ phase.

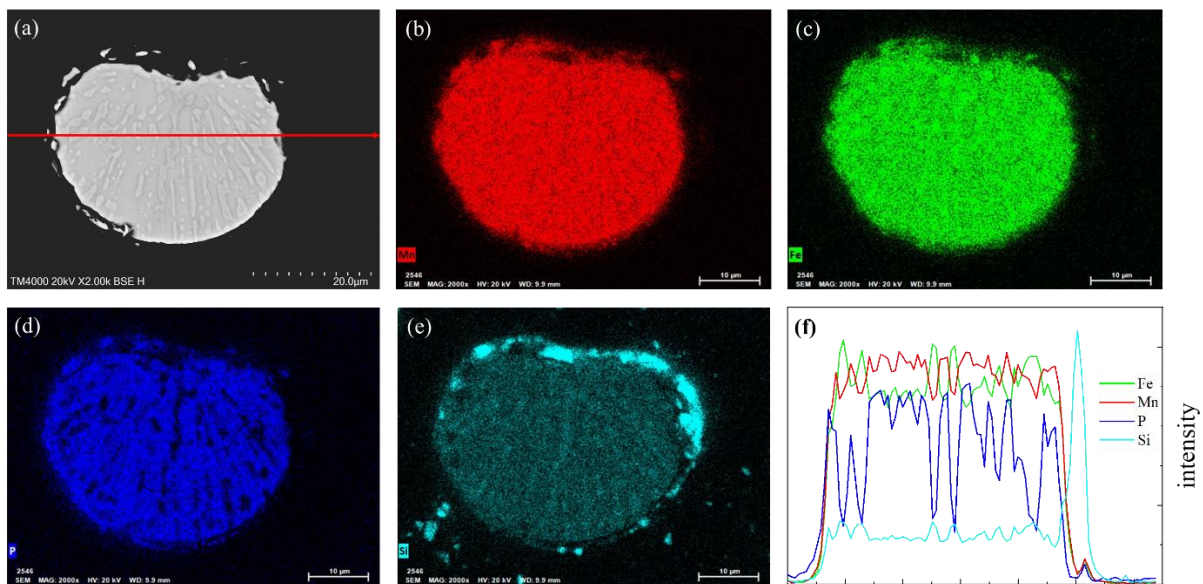


Fig. 2(a) The SEM image, (b-e) EDS color maps, and (f) line scans along the direction of the red arrow of the cross section for the $\text{Mn}_{1.0}\text{Fe}_{1.0}\text{P}_{0.5}\text{Si}_{0.5}$ microwire.

Table 1. The compositions of the two phases in $\text{Mn}_x\text{Fe}_{2-x}\text{P}_{0.5}\text{Si}_{0.5}$ microwires

x	Main phase		Impurity	
	composition	M/NM	composition	M/NM
0.7	$\text{Mn}_{27.5}\text{Fe}_{40.8}\text{P}_{19.1}\text{Si}_{12.7}$	2.15	$\text{Mn}_{19.6}\text{Fe}_{56.1}\text{P}_{3.7}\text{Si}_{20.5}$	3.14
0.8	$\text{Mn}_{30.3}\text{Fe}_{38.2}\text{P}_{18.1}\text{Si}_{13.4}$	2.18	$\text{Mn}_{23.0}\text{Fe}_{51.6}\text{P}_{4.6}\text{Si}_{20.8}$	2.94
0.9	$\text{Mn}_{32.9}\text{Fe}_{35.2}\text{P}_{19.0}\text{Si}_{12.9}$	2.14	$\text{Mn}_{27.1}\text{Fe}_{48.0}\text{P}_{4.5}\text{Si}_{20.5}$	3.01
1.0	$\text{Mn}_{36.5}\text{Fe}_{30.7}\text{P}_{20.0}\text{Si}_{12.8}$	2.05	$\text{Mn}_{30.8}\text{Fe}_{43.9}\text{P}_{4.9}\text{Si}_{20.3}$	2.96
1.1	$\text{Mn}_{39.7}\text{Fe}_{28.5}\text{P}_{18.5}\text{Si}_{13.4}$	2.14	$\text{Mn}_{37.0}\text{Fe}_{35.6}\text{P}_{8.3}\text{Si}_{19.1}$	2.64
1.2	$\text{Mn}_{42.3}\text{Fe}_{25.4}\text{P}_{19.6}\text{Si}_{12.7}$	2.10	$\text{Mn}_{39.0}\text{Fe}_{36.8}\text{P}_{2.8}\text{Si}_{21.5}$	3.12

Figure 3 shows the phase map and IPF map obtained by EBSD measurements of the $\text{Mn}_{1.0}\text{Fe}_{1.0}\text{P}_{0.5}\text{Si}_{0.5}$ microwire. The phase distribution can be seen clearly from the phase map, as shown in Fig. 3(a). The $(\text{Mn, Fe})_3\text{Si}$ phase was dispersed throughout the cross-section, no segregation occurred. Fig. 3(b) displays the micron-size grain without preferential orientation.

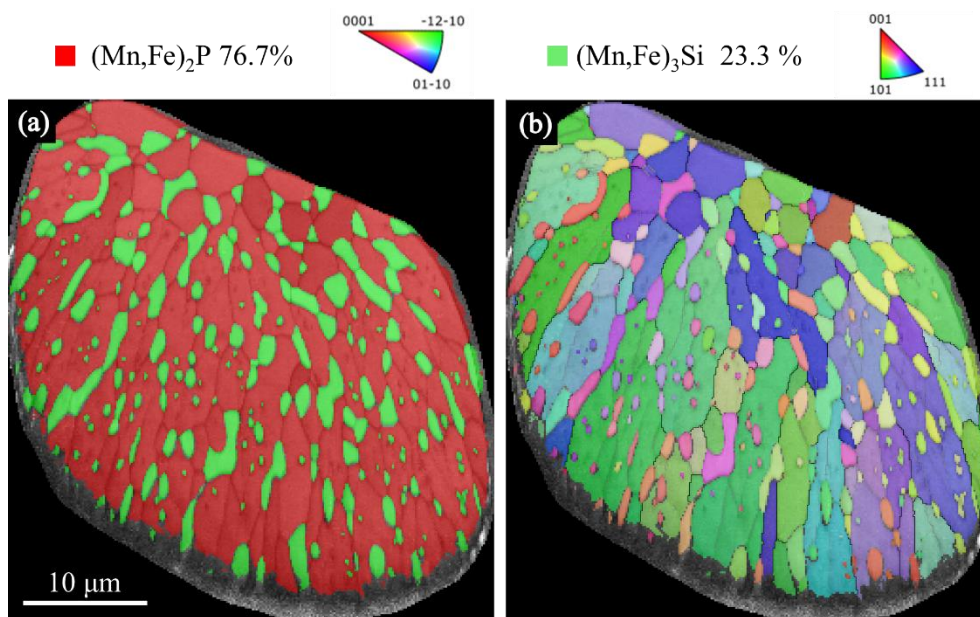


Fig. 3. EBSD analysis: (a) Phase map and (b) IPF map of the $\text{Mn}_{1.0}\text{Fe}_{1.0}\text{P}_{0.5}\text{Si}_{0.5}$ microwire.

The high-angle annular dark field (HAADF) image of the $\text{Mn}_{1.0}\text{Fe}_{1.0}\text{P}_{0.5}\text{Si}_{0.5}$ microwire, as shown in Fig. 4(a), confirmed that the crystallite size is in the micron range. Figs. 4(b) and (d) show the high-resolution TEM (HRTEM) images of grain A and B in Fig. 4(a). The grain A and B are confirmed in the hexagonal Fe_2P -type structure (space group $P\bar{6}2m$) and cubic

Fe_3Si -type structure (space group $Fm\bar{3}m$) respectively by performing the fast Fourier transform (FFT) of the corresponding HRTEM images, as shown in Fig. 4(c) and (e). The zone axis is identified to be [001] for both grains. Figs 4(f-i) show the corresponding energy dispersive spectroscopy (EDS) maps for Mn, Fe, P, and Si of Fig. 4(a), confirming that more Fe and Si atoms are present with negligible P atoms in the $(\text{Mn,Fe})_3\text{Si}$ phase.

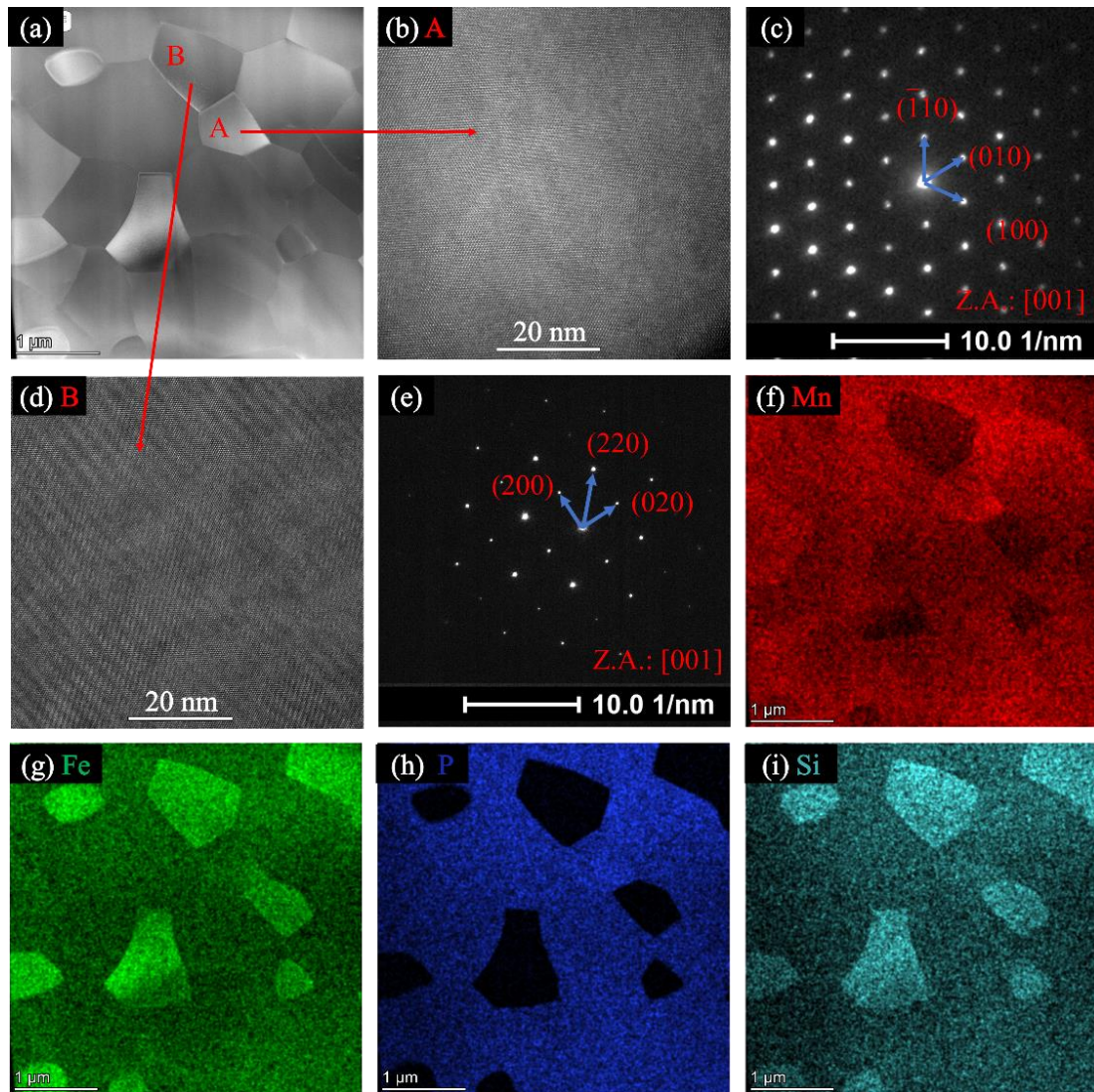


Fig. 4. (a) The high-angle annular dark field (HAADF) image, HRTEM images and the FFT for the grains (b, c) A and (d, e) B, (f-i) TEM-EDS maps of the $\text{Mn}_{1.0}\text{Fe}_{1.0}\text{P}_{0.5}\text{Si}_{0.5}$ microwire.

Magnetic and magnetocaloric properties

A PPMS paired with the vibrating sample magnetometer (VSM) option was utilized to characterize the magnetic properties of the microwires. The temperature-dependent magnetization (M - T) curves, the Mn-content dependence of the Curie temperature (T_C) and thermal hysteresis (T_{hys}), for $\text{Mn}_x\text{Fe}_{2-x}\text{P}_{0.5}\text{Si}_{0.5}$ microwires under a magnetic field of 0.05 T are displayed in Fig. 5. The deduced magnetic parameters are listed in Table 2. All the M - T curves show an FM-PM transition, with thermal hysteresis observed between field-warming (FW) and field-cooling (FC) curves. For $x=0.7$, the Curie temperature exceeds 400 K, which is above the experimental temperature range available. The T_C was found to decrease from 351 to 190 K as the Mn content x increased from 0.8 to 1.2. The decrease in T_C could be mainly caused by the changes in the Mn/Fe ratio. In addition, the T_{hys} increased from 14.5 to 22 K as the Mn content x increased.

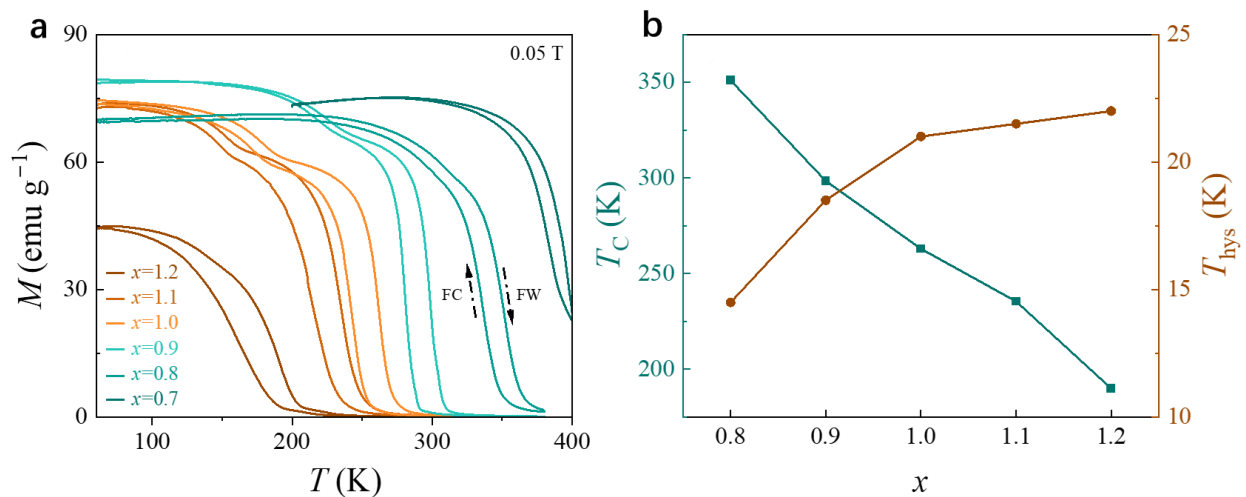


Fig. 5 (a) The temperature dependence of magnetization under FW and FC measurement protocols, (b) the Curie temperature and thermal hysteresis of $\text{Mn}_x\text{Fe}_{2-x}\text{P}_{0.5}\text{Si}_{0.5}$ microwires.

Table 2. The magnetic and magnetocaloric properties of $\text{Mn}_x\text{Fe}_{2-x}\text{P}_{0.5}\text{Si}_{0.5}$ microwires

x	T_C (K)	T_{hys} (K)	W_y^{peak} (J kg^{-1})	$\Delta S_{\text{iso}}^{\text{peak}}$ ($\text{J kg}^{-1} \text{K}^{-1}$)	RC (J kg^{-1})	RCE (J kg^{-1})
0.7	> 400	-	-	-	-	-
0.8	351	14.5	19.6	12.0	293.7	279.2
0.9	298.5	18.5	60.7	18.3	331.1	284.6
1.0	263	21	58.4	15.8	300	257.1
1.1	235.5	21.5	28.7	10.9	280.9	262.3
1.2	190	22	28.9	7.9	288.4	267.5

Figure 6a displays the isothermal magnetization curves of $\text{Mn}_{1.0}\text{Fe}_{1.0}\text{P}_{0.5}\text{Si}_{0.5}$ microwires under applied magnetic fields ranging from 0-5 T. The non-coincidence of magnetization and demagnetization M - H curves in Fig. 6a indicates the existence of magnetic hysteresis around the T_C , arising from the type of the first-order phase transition that occurs in the microwires. The magnetic hysteresis loss (W_y) is defined as the area between the magnetization and demagnetization curves.^[33] Accordingly, the temperature dependence of W_y for $\text{Mn}_x\text{Fe}_{2-x}\text{P}_{0.5}\text{Si}_{0.5}$ microwires is estimated, and the results are shown in Fig. 6b. Larger values of W_y were found for $x = 0.9$ and 1.0 , in which the Mn/Fe ratio of the Fe_2P phase trends towards 1, while the other samples show smaller magnetic hysteresis losses.

The isothermal magnetic entropy change (ΔS_{iso}), which is one of the important parameters for evaluating the magnetocaloric effect of a magnetic material, was calculated using the isothermal magnetization data (e.g., Fig. 4a), via Maxwell equation, i.e., eq. (1):

$$\Delta S_{\text{iso}} = \mu_0 \int_0^H \left(\frac{\partial M}{\partial T} \right)_{H'} dH' \quad (1)$$

Figure 6c shows a plot of variation of isothermal magnetic entropy change with temperature for $\text{Mn}_x\text{Fe}_{2-x}\text{P}_{0.5}\text{Si}_{0.5}$ microwires for a field change of 5 T. It can be seen in this

figure that the peak value of ΔS_{iso} increased from 7.9 to 18.3 $\text{J kg}^{-1} \text{K}^{-1}$ with decreasing x from 1.2 to 0.9, maximized at $x=0.9$, and then decreased to 12.0 as x continued to decrease to 0.8. This changing trend in ΔS_{iso} can be attributed to the change in the Mn/Fe ratio and hence the fraction of the Fe_2P phase. Interestingly, the largest value of ΔS_{iso} is achieved near room temperature for the $x=0.9$ composition.

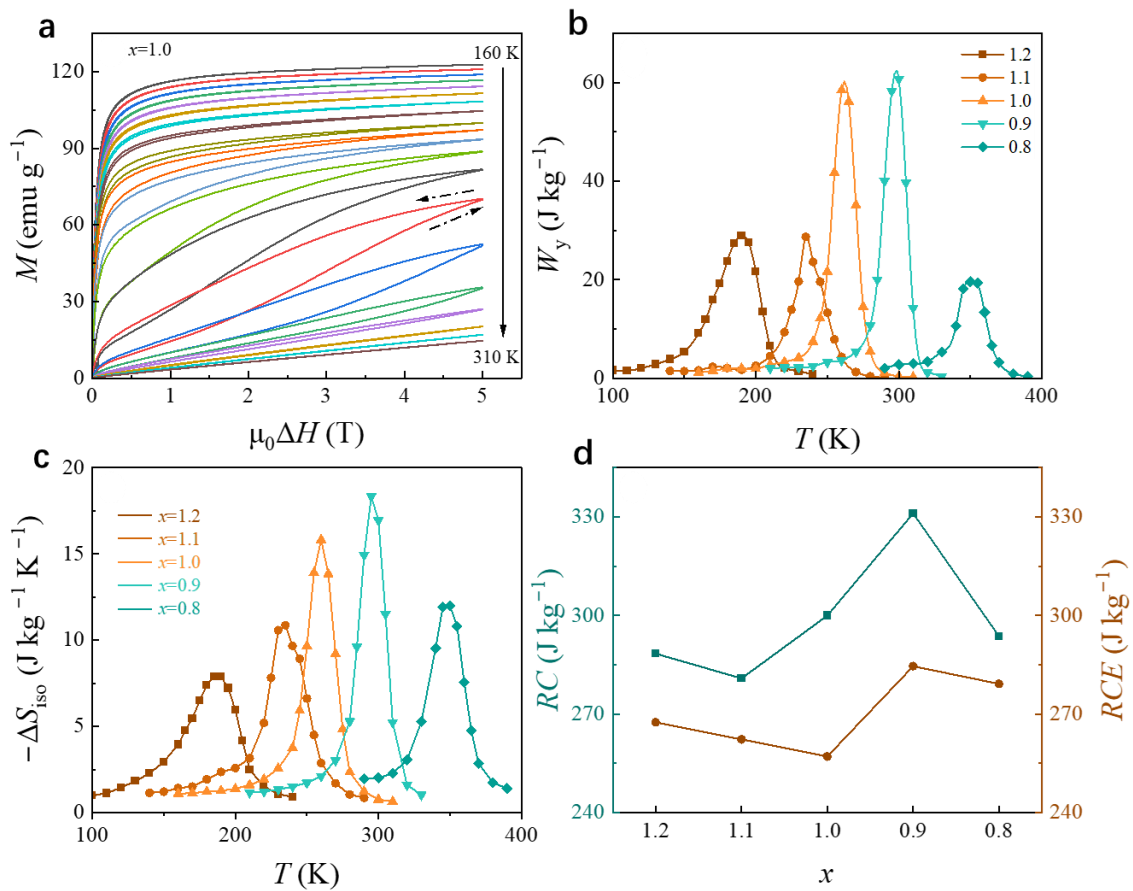


Fig. 6 (a) The isothermal magnetization M - H curves of $\text{Mn}_{1.0}\text{Fe}_{1.0}\text{P}_{0.5}\text{Si}_{0.5}$ ($x=1.0$) microwires, (b) the magnetic hysteresis loss (W_y), (c) the isothermal magnetic entropy change (ΔS_{iso}), (d) refrigerant capacity (RC) and effective refrigerant capacity (RCE) of $\text{Mn}_x\text{Fe}_{2-x}\text{P}_{0.5}\text{Si}_{0.5}$ microwires for a field change of 5 T.

In addition to the isothermal magnetic entropy change, the refrigerant capacity (RC) is another important parameter for the evaluation of the cooling efficiency of magnetocaloric

materials. The RC is determined by the integral area in the temperature range of full width at half maximum under the $\Delta S_{iso}-T$ curves^[12], i.e., Eq. (2):

$$RC = \int_{T_1}^{T_2} -\Delta S_{iso}(T) dT, \quad (2)$$

where T_1 and T_2 are the corresponding temperatures of half maximum of isothermal magnetic entropy change, and $T_1 \leq T_2$. Taking the magnetic hysteresis losses into account, the RC values after subtracting the average magnetic hysteresis loss (ΔW_y) are referred as to the effective refrigerant capacity (RCE) values. The ΔW_y is determined by the averaging integral area under the W_y-T curves using the same integration limit as RC ^[28,33], i.e., Eq. (3):

$$\Delta W_y = \frac{\int_{T_1}^{T_2} W_y(T) dT}{T_2 - T_1} \quad (3)$$

The RC and RCE values obtained for $Mn_xFe_{2-x}P_{0.5}Si_{0.5}$ microwires for a field change of 5 T are plotted versus the Mn content, as shown in Fig. 6(d). By varying the Mn content, the RC shows a similar trend as ΔS_{iso} except for $x=1.2$. In comparison with the $x=1.1$ sample, the $x=1.2$ sample shows the larger RC , and the latter possesses a smaller ΔS_{iso} value than the former. This could be attributed to the broader FM-PM transition for the $x=1.2$ sample as compared to the $x=1.1$ sample. The largest RC and RCE values (331.1 and 284.6 J kg⁻¹, respectively) are also achieved for the $x=0.9$ sample. The magnetic and magnetocaloric properties of the $Mn_xFe_{2-x}P_{0.5}Si_{0.5}$ ($x=0.9$) microwires (MW-1 h) and their bulk counterparts (Figs. S1 and S1 in Supporting Information) are listed in Table 3. It can be seen in this table that one bulk counterpart under the same heat-treatment (B-1 h) showed a larger ΔS_{iso} but a similar RCE . Another bulk counterpart, subjected to the heat treatment for 4 days (B-4 d), showed a decreased RCE despite an increase in ΔS_{iso} , due to its increased hysteresis loss. These values of ΔS_{iso} are much larger than those achieved for Gd-based microwires with much lower T_C values

[9-15], and for the magnetocaloric materials with T_C around 300 K (see Table 3). These results indicate that the $Mn_xFe_{2-x}P_{0.5}Si_{0.5}$ ($x=0.9$) microwires are very compelling candidates for active magnetic refrigeration in the room temperature regime.

Table 3. The magnetic and magnetocaloric properties of magnetocaloric materials

Materials	T_C (K)	T_{hys} (K)	W_y^{peak} (J kg ⁻¹)	ΔS_{iso}^{peak} (J kg ⁻¹ K ⁻¹)	RC (J kg ⁻¹)	RCE (J kg ⁻¹)	Ref.
MW-1 h	298.5	18.5	60.7	18.3	331.1	284.6	This work
B-1 h	350	13	18.1	6.6	305.9	293.2	This work
B-4 d	319	33.5	155.6	22.4	360.1	242.3	This work
$Mn_{1.20}Fe_{0.75}P_{0.45}Si_{0.55}$	301.5	1	-	11.9	-	-	[34]
$MnFeP_{0.5}Si_{0.5}$	282	40	-	18.1	-	-	[35]
Gd	290	-	-	9.8	-	-	[36]
$LaFe_{11.5}Al_{1.5}H_{1.3}$	295	-	-	12.3	-	-	[37]
$Ni_{52.9}Mn_{22.4}Ga_{24.7}$	305	-	-	8.6	-	-	[38]

Conclusions

We have successfully created a novel class of $Mn_xFe_{2-x}P_{0.5}Si_{0.5}$ microwires with tunable giant magnetocaloric properties around room temperature, by harnessing the combined advantages of melt-extraction, thermal treatment, and chemical engineering. The $Mn_xFe_{2-x}P_{0.5}Si_{0.5}$ microwires crystallize into an Fe_2P -type structure as a majority phase, with $(Mn,Fe)_3Si$ present as an impurity phase whose volume fraction decreases with increasing Mn content. By varying the Mn content x from 0.8 to 1.2, the Curie temperature (T_C) can be adjusted from 351 to 190 K while the thermal hysteresis (T_{hys}) can be altered between 15 and 22 K. Among the compositions investigated, the largest values of ΔS_{iso} , RC , and RCE (18.3 J kg⁻¹ K⁻¹, 331.1 and 284.6 J kg⁻¹, respectively) are achieved for $x=0.9$ at ambient temperature. The adjustability of the microstructural and magnetic properties combined with a short-time heat treatment

identifies melt-extracted Mn-Fe-P-Si microwires as a strong candidate for active magnetic refrigeration at room temperature.

Methods

Fabrication

$\text{Mn}_x\text{Fe}_{2-x}\text{P}_{0.5}\text{Si}_{0.5}$ ($0.7 \leq x \leq 1.2$) microwires of ~ 50 μm diameter were prepared by melt-extraction, followed by subsequent heat-treatment. First, an 8 mm diameter rod was prepared by arc-melting and casting. The raw materials were crystals of Mn (99.5 %), Fe (99.99 %), FeP chunks (98 %), and Si (99.999 %). An excess of 5 wt.% of Mn was added to compensate for the loss during arc-melting. Then, the rod was placed in a homemade melt-extractor system to be transformed into microwires.^[30] Finally, the as-prepared microwires were sealed in a quartz tube under 30 KPa Ar atmosphere and annealed at 1323 K for 1 h and then water quenched.

Structural and magnetic characterization

The microwires were ground into powders for X-ray diffraction (XRD) characterization, and the XRD patterns of the powdered samples were collected from 30 to 90° on a PANalytical X'Pert Pro diffractometer (Empyrean) with Cu-K α radiation at room temperature. Rietveld refinement was performed using Fullprof program for obtaining the structural parameters and phase fractions. Microstructural and compositional information were obtained using a scanning electron microscope (SEM, TM4000) with energy dispersive spectrometer (EDS). Electron back-scatter diffraction (EBSD) and transmission electron microscopy (TEM) measurements were also performed on a field emission scanning electron microscope (Gemini560) and a FEI Talos F200X system, respectively. Magnetic measurements were carried out on a Quantum Design Physical Property Measurement System (PPMS-16 T).

Data availability. The data that support the findings of this study are available from the corresponding author on a reasonable request.

Acknowledgments

Research at HIT was funded by the National Natural Science Foundation of China (NSFC, Nos. 51871124), grant PID2019-105720RB-I00 funded by MCIN/AEI /10.13039/501100011033. M.H.P acknowledges support from the University of South Florida under Grant No. 125300. Noah Schulz is acknowledged for proofreading the manuscript.

Author contributions

L.L. and H.X.S. initiated the research. L.L., H.X.S., L.Y.Z., Y.J.H., J.F.S. participated in the structural and magnetic experiments. L.L., H.X.S. and M.H.P. analyzed the data. L.L., H.X.S. and M.H.P. prepared the first draft of the manuscript and all the co-authors contributed to the final version of the manuscript. J.F.S. led the project.

Competing interests: The authors declare no conflict of interest.

REFERENCES

1. A. Kitanovski. Energy Applications of Magnetocaloric Materials. *Adv. Energy Mater.* **2020**, *10*, 1903741, doi: 10.1002/aenm.201903741.
2. P.V. Trevizoli; J.R. Barbosa. Overview on Magnetic Refrigeration. In *Encyclopedia of Smart Materials*; Olabi, A., Ed.; Elsevier: Oxford, 2022, pp. 395-406.
3. M.H. Phan; S.C. Yu. Review of the magnetocaloric effect in manganite materials. *J. Magn. Magn. Mater.* **2007**, *308*, 325-340, doi: 10.1016/j.jmmm.2006.07.025.
4. V. Franco; J.S. Blázquez; J.J. Ipus; J.Y. Law; L.M. Moreno-Ramírez; A. Conde. Magnetocaloric effect: from materials research to refrigeration devices. *Prog. Mater. Sci.* **2018**, *93*, 112-232, doi: 10.1016/j.pmatsci.2017.10.005.
5. K.A. Gschneidner; V.K. Pecharsky. Thirty years of near room temperature magnetic cooling: Where we are today and future prospects. *International Journal of Refrigeration* **2008**, *31*, 945-961, doi: 10.1016/j.ijrefrig.2008.01.004.
6. A. Smith; C.R.H. Bahl; R. Bjørk; K. Engelbrecht; K.K. Nielsen; N. Pryds. Materials challenges for high performance magnetocaloric refrigeration devices. *Adv. Energy Mater.* **2012**, *2*, 1288-1318, doi: 10.1002/aenm.201200167.
7. M.D. Kuz'Min. Factors limiting the operation frequency of magnetic refrigerators. *Appl. Phys. Lett.* **2007**, *90*, 251916, doi: 10.1063/1.2750540.
8. D. Vuarnoz; T. Kawanami. Numerical analysis of a reciprocating active magnetic regenerator made of gadolinium wires. *Appl. Therm. Eng.* **2012**, *37*, 388-395, doi: 10.1016/j.applthermaleng.2011.11.053.
9. F.X. Qin; N.S. Bingham; H. Wang; H.X. Peng; J.F. Sun; V. Franco; S.C. Yu; H. Srikanth;

- M.H. Phan. Mechanical and magnetocaloric properties of Gd-based amorphous microwires fabricated by melt-extraction. *Acta Mater.* **2013**, *61*, 1284-1293, doi: 10.1016/j.actamat.2012.11.006.
10. H.F. Belliveau; Y.Y. Yu; Y. Luo; F.X. Qin; H. Wang; H.X. Shen; J.F. Sun; S.C. Yu; H. Srikanth; M.H. Phan. Improving mechanical and magnetocaloric responses of amorphous melt-extracted Gd-based microwires via nanocrystallization. *J. Alloy. Compd.* **2017**, *692*, 658-664, doi: 10.1016/j.jallcom.2016.08.254.
 11. H.X. Shen; D.W. Xing; J.L. Sánchez Llamazares; C.F. Sánchez-Valdés; H. Belliveau; H. Wang; F.X. Qin; Y.F. Liu; J.F. Sun; H. Srikanth; M.H. Phan. Enhanced refrigerant capacity in Gd-Al-Co microwires with a biphasic nanocrystalline/amorphous structure. *Appl. Phys. Lett.* **2016**, *108*, doi: 10.1063/1.4943137.
 12. N.T.M. Duc; H.X. Shen; E.M. Clements; O. Thiabgoh; J.L. Sanchez Llamazares; C.F. Sanchez-Valdes; N.T. Huong; J.F. Sun; H. Srikanth; M.H. Phan. Enhanced refrigerant capacity and Curie temperature of amorphous Gd₆₀Fe₂₀Al₂₀ microwires. *J. Alloy. Compd.* **2019**, *807*, 151694, doi: <https://doi.org/10.1016/j.jallcom.2019.151694>.
 13. Y.F. Wang; F.X. Qin; Y. Luo; H. Wang; H.X. Peng. Tuning of magnetocaloric effect and optimization of scaling factor for Gd₅₅Ni₁₀Co₃₅ amorphous microwires. *J. Alloy. Compd.* **2018**, *761*, 1-7, doi: 10.1016/j.jallcom.2018.05.152.
 14. N.T.M. Duc; H.X. Shen; O. Thiabgoh; N.T. Huong; J.F. Sun; M.H. Phan. Melt-extracted Gd_{73.5}Si₁₃B_{13.5}/GdB₆ ferromagnetic/antiferromagnetic microwires with excellent magnetocaloric properties. *J. Alloy. Compd.* **2020**, *818*, 153333, doi: 10.1016/j.jallcom.2019.153333.

15. Y. Wang; N. Thi My Duc; T. Feng; H. Wei; F. Qin; M. Phan. Competing ferromagnetic and antiferromagnetic interactions drive the magnetocaloric tunability in Gd₅₅Co₃₀Ni_xAl_{15-x} microwires. *J. Alloy. Compd.* **2022**, *907*, 164328, doi: 10.1016/j.jallcom.2022.164328.
16. H. Zhang; M. Qian; X. Zhang; S. Jiang; L. Wei; D. Xing; J. Sun; L. Geng. Magnetocaloric effect of Ni-Fe-Mn-Sn microwires prepared by melt-extraction technique. *Materials & Design* **2017**, *114*, 1-9, doi: 10.1016/j.matdes.2016.10.077.
17. R. Varga; T. Ryba; Z. Vargova; S. Michalik; V. Zhukova; A. Zhukov; J.L. Sanchez Llamazares; A. Quintana-Nedelcos. Magnetocaloric effects in magnetic microwires for magnetic refrigeration applications. In *Magnetic Nano- and Microwires*; Vázquez, M., Ed.; Woodhead Publishing, 2015, pp. 569-587.
18. M. Qian; X. Zhang; L. Wei; P. Martin; J. Sun; L. Geng; T.B. Scott; H. Peng. Tunable Magnetocaloric Effect in Ni-Mn-Ga Microwires. *Sci. Rep.-Uk* **2018**, *8*, 16574-16578, doi: 10.1038/s41598-018-35028-9.
19. H. Zhang; X. Zhang; M. Qian; L. Yin; L. Wei; D. Xing; J. Sun; L. Geng. Magnetocaloric effect in Ni-Fe-Mn-Sn microwires with nano-sized γ precipitates. *Appl. Phys. Lett.* **2020**, *116*, doi: 10.1063/1.5132767.
20. X.F. Miao; S.Y. Hu; F. Xu; E. Brück. Overview of magnetoelastic coupling in (Mn, Fe)₂(P, Si)-type magnetocaloric materials. *Rare Metals* **2018**, *37*, 723-733, doi: 10.1007/s12598-018-1090-2.
21. T. Gottschall; K.P. Skokov; M. Fries; A. Taubel; I. Radulov; F. Scheibel; D. Benke; S. Riegg; O. Gutfleisch. Making a Cool Choice: The Materials Library of Magnetic

- Refrigeration. *Adv. Energy Mater.* **2019**, *9*, 1901322, doi: 10.1002/aenm.201901322.
22. F. Zhang; S. Smits; A. Kiecana; I. Batashev; Q. Shen; N. van Dijk; E. Brück. Impact of W doping on Fe-rich (Mn,Fe)₂(P,Si) based giant magnetocaloric materials. *J. Alloy. Compd.* **2023**, *933*, 167802, doi: <https://doi.org/10.1016/j.jallcom.2022.167802>.
 23. Z. Zheng; H. Wang; C. Li; X. Chen; D. Zeng; S. Yuan. Enhancement of Magnetic Properties and Magnetocaloric Effects for Mn_{0.975}Fe_{0.975}P_{0.5}Si_{0.5} Alloys by Optimizing Quenching Temperature. *Adv. Eng. Mater.* **2022**, *2200160*, doi: 10.1002/adem.202200160.
 24. A. He; V. Svitlyk; Y. Mozharivskyj. Synthetic Approach for (Mn,Fe)₂(Si,P) Magnetocaloric Materials: Purity, Structural, Magnetic, and Magnetocaloric Properties. *Inorg. Chem.* **2017**, *56*, 2827-2833, doi: 10.1021/acs.inorgchem.6b02912.
 25. L. Luo; J.Y. Law; H. Shen; L.M. Moreno-Ramírez; V. Franco; S. Guo; N.T.M. Duc; J. Sun; M. Phan. Enhanced Magnetocaloric Properties of Annealed Melt-Extracted Mn_{1.3}Fe_{0.6}P_{0.5}Si_{0.5} Microwires. *Metals* **2022**, *12*, 1536, doi: 10.3390/met12091536.
 26. X. You; M. Maschek; N.H.H. van Dijk; E. Brück. Magnetic Phase Diagram of the Mn_xFe_{2-x}P_{1-y}Si_y System. *Entropy-Switz.* **2022**, *24*, 2, doi: 10.3390/e24010002.
 27. D. Fruchart; S. Haj-Khlifa; P. de Rango; M. Balli; R. Zach; W. Chajec; P. Fornal; J. Stanek; S. Kaprzyk; J. Tobola. Structure and Magnetic Properties of Bulk Synthesized Mn_{2-x}Fe_xP_{1-y}Si_y Compounds from Magnetization, ⁵⁷Fe Mössbauer Spectroscopy, and Electronic Structure Calculations. *Crystals* **2019**, *9*, 37, doi: 10.3390/cryst9010037.
 28. Z.G. Zheng; W.H. Wang; Q. Zhou; L. Lei; Y. Hong; D.C. Zeng; Y. Mozharivskyj. Microstructure and magnetocaloric effects of Mn_{1.2}Fe_{0.8}P_{0.6}Si_{0.4}B_{0.05} alloys prepared by ball milling and spinning methods. *J. Magn. Magn. Mater.* **2019**, *477*, 203-208, doi:

10.1016/j.jmmm.2019.01.053.

29. G.F. Wang; B.Y. Yang; T. Jing; Z.R. Zhao; X.F. Zhang; Y.L. Liu. A Comparative Study of the Magnetocaloric Effect in MnFePSiGeB Prepared by Traditional Sintering and Spark Plasma Sintering. *Ieee T. Magn.* **2019**, *55*, 1-5, doi: 10.1109/TMAG.2018.2868451.
30. H. Shen; H. Wang; J. Liu; D. Xing; F. Qin; F. Cao; D. Chen; Y. Liu; J. Sun. Enhanced magnetocaloric and mechanical properties of melt-extracted Gd₅₅Al₂₅Co₂₀ micro-fibers. *J. Alloy. Compd.* **2014**, *603*, 167-171, doi: 10.1016/j.jallcom.2014.03.053.
31. O. Tegus; K. Koyama; J.L. Her; K. Watanabe; E. Brück; K.H.J. Buschow; F.R. de Boer. X-ray diffraction on MnFeP_{0.46}As_{0.54} in a magnetic field. *Physica B: Condensed Matter* **2007**, *392*, 151-153, doi: 10.1016/j.physb.2006.11.010.
32. G.F. Wang; Z.R. Zhao; L. Song; O. Tegus. Peculiar influence of Mn/Fe ratio on the magnetic and magnetocaloric properties of Mn_{2-x}Fe_xP_{0.6}Si_{0.25}Ge_{0.15} compounds. *J. Alloy. Compd.* **2013**, *554*, 208-213, doi: 10.1016/j.jallcom.2012.11.075.
33. S. Kavita; M. Alagusoundarya; V.V. Ramakrishna; V. Suresh; P. Bhatt; P. Srimathi; R. Archana; D. Kar; T. Thomas; R. Gopalan. On the table-like magnetocaloric effect, microstructure and mechanical properties of La_xFe_{11.6}Si_{1.4} system. *J. Alloy. Compd.* **2022**, *895*, doi: 10.1016/j.jallcom.2021.162597.
34. D. Tu; J. Li; Z. Dong; L. Zeng; M. Xia; Q. Hu; J. Li. Effect of heat treatment on microstructure evolution and magnetocaloric properties of droplet melted Mn-Fe-P-Si alloys. *Journal of Materials Research and Technology* **2022**, *20*, 1593-1602, doi: 10.1016/j.jmrt.2022.07.178.
35. C.F. Li; Z.G. Zheng; W.H. Wang; J.Y. Liu; L. Lei; D.C. Zeng. Effect of M/NM ratios on

- structural and magnetic properties of $(\text{Mn,Fe})_2(\text{P,Si})$ compounds. *Physica B: Condensed Matter* **2020**, 594, 412309, doi: 10.1016/j.physb.2020.412309.
36. V.K. Pecharsky; K.A. Gschneidner. Giant Magnetocaloric Effect in $\text{Gd}_5\text{Si}_2\text{Ge}_2$. *Phys. Rev. Lett.* **1997**, 78, 4494-4497.
37. J.L. Zhao; J. Shen; B.G. Shen; F.X. Hu; J.R. Sun. Enhancement of the magnetocaloric effect and magnetic transition temperature in $\text{LaFe}_{11.5}\text{Al}_{1.5}$ by hydrogenation. *Solid State Commun.* **2010**, 150, 2329-2332, doi: 10.1016/j.ssc.2010.10.006.
38. X. Zhou; W. Li; H.P. Kunkel; G. Williams; S. Zhang. Relationship between the magnetocaloric effect and sequential magnetic phase transitions in Ni-Mn-Ga alloys. *J. Appl. Phys.* **2005**, 10M-515M.